AEM
Journals.ASM.org

Silicon and Phosphorus Linkage with Iron via Oxygen in the Amorphous Matrix of *Gallionella ferruginea* Stalks

Tomoko Suzuki, Hideki Hashimoto, Atsushi Itadani, Nobuyuki Matsumoto, Hitoshi Kunoh, and Jun Takada

Graduate School of Natural Science and Technology, Okayama University, Okayama, Japan

Bacterial species belonging to the genus *Gallionella* are Fe-oxidizing bacteria that produce uniquely twisted extracellular stalks consisting of iron-oxide-encrusted inorganic/organic fibers in aquatic environments. This paper describes the degree of crystallinity of *Gallionella* stalks and the chemical linkages of constituent elements in the stalk fibers. Transmission electron microscopy revealed that the matrix of the fiber edge consisted of an assembly of primary particles of approximately 3 nm in diameter. Scanning transmission electron microscopy revealed the rough granular surfaces of the fibers, which reflect the disordered assembly of the primary particles, indicating a high porosity and large specific surface area of the fibers. This may provide the surface with broader reactive properties. X-ray diffractometry, selected-area electron diffraction, and high-resolution transmission electron microscopy together showed that the primary particles had an amorphous structure. Furthermore, energy-dispersive X-ray analysis and Fourier transform infrared spectroscopy detected the bands characteristic of the vibrational modes assigned to O-H, Fe-O-H, P-O-H, Si-O-H, Si-O-Fe, and P-O-Fe bonds in the stalks, suggesting that the minor constituent elements P and Si could affect the degree of crystallinity of the fibers by linking with Fe via O. This knowledge about the mutual associations of these elements provides deeper insights into the unique inorganic/organic hybrid structure of the stalks.

Iron has long been recognized as a potential energy source for certain bacteria (16). *Gallionella ferruginea*, an iron-oxidizing bacterium, has been considered to depend on Fe(II) oxidation as an electron source for autotrophic growth (23). Biotic and/or abiotic depositions of the oxidized form Fe(III) give rise to extracellular, ferric oxide-encrusted, spirally twisted stalks (18, 21). The *Gallionella* cells and associated stalks are found ubiquitously in various aquatic environments such as iron seeps (1), creeks (15), groundwater (30), drinking-water distribution systems (35, 44), wetland rhizospheres (56), and acid mine drainage (3).

Bacterial cells and their surfaces have been often reported as nucleation sites for both metal sulfides and complex polymorphic (Fe, Al) silicates (19, 53). Typical examples are Fe-oxidizing bacteria such as *Gallionella*, *Leptothrix*, *Mariprofundus*, and *Rhodobacter* (5, 21, 26, 41, 47, 51, 55), which are known to have an ability to form extracellular Fe-rich stalks or sheaths. The elements precipitated in such structures are largely affected by the aquatic environments that the bacteria inhabit. According to Ridgway and Olson (44), the stalks of *Gallionella* found on pipe surfaces in drinking water distribution systems contain a large quantity of Fe, Si, Al, and Ca and traces of P and S. On the other hand, the stalks from a lake metalimnion were found to contain Fe, Si, Ca, and S but not Al and P (27). Our previous scanning electron microscopy (SEM) and scanning transmission electron microscopy (STEM)/energy-dispersive X-ray (EDX) analyses (52) demonstrated an almost uniform distribution of Fe, O, Si, and P in *Gallionella* stalks collected from a water purification system, as was similarly found in *Leptothrix ochracea* sheaths (47). It has been reported that Fe exists in stalk fibers in the form of FeOOH, α-FeOOH (4, 5, 6, 33), $Fe(OH)_3$ (20), 2-line ferrihydrite (33, 57), or Fe_2O_3 (24). Chan et al. (6) analyzed the biofilms found in the cloudy water of flooded underground tunnels (consisting predominantly of ferrihydrite- and goethite-encrusted sheaths and stalks characteristic of *Leptothrix* sp. and *Gallionella ferruginea*, respectively) by microscopy and spectroscopy. They found that the biofilm filaments from the cloudy water consisted of amorphous iron oxyhydroxide and that each filament contained one thin, pseudosingle crystal core surrounded by a porous layer of nanocrystalline 2-line ferrihydrite. In contrast to the accumulated data on Fe forms, our understanding about the constitutional elements other than Fe, specifically the nature of the interaction of Si, P, and/or other minor elements with Fe and/or O in the structures, is limited. As far as we know, the only published information available is the hypothesis by Kennedy et al. (32) for silicified iron oxides in *Gallionella* stalks, which states that adsorbed water might be replaced by adsorbed Si in the form of Fe-O-Si bonds. We believe that chemical linkages of these minor elements such as Si and P with Fe and O must be closely associated with the degree of crystallinity of the stalk and sheath matrices because it is known that inorganic ligands such as SiO_4 and PO_4 in Fe(III) hydrolysates interfere with the polymerization and crystallization of Fe oxyhydroxide precipitates (9, 11, 46).

With this in mind, we have in this study attempted to analyze the basic surface structures of the *Gallionella* stalk by STEM, and the degree of crystallinity of its matrix by X-ray diffractometry (XRD), selected-area electron diffraction (SAED), and high-resolution transmission electron microscopy (HRTEM). The elemental constituents and the nature of their chemical associations in the matrix were analyzed by EDX analysis and Fourier transform infrared (FTIR) spectroscopy.

MATERIALS AND METHODS

Sample collection and specimen preparation for electron microscopy. Ocherous flocs associated with microbial mats attached to the wall of a

Received 21 June 2011 **Accepted** 14 October 2011
Published ahead of print 21 October 2011
Address correspondence to Jun Takada, jtakada@cc.okayama-u.ac.jp.
Supplemental material for this article may be found at http://aem.asm.org/.

doi:10.1128/AEM.05913-11

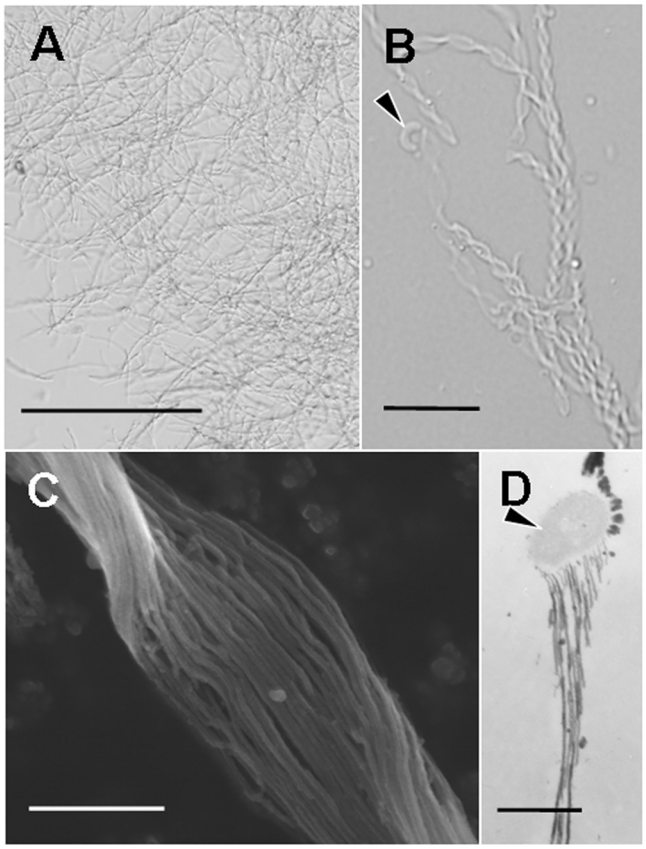

FIG 1 Micrographs of *G. ferruginea* twisted stalks. (A) The assembled stalks in the ocherous precipitates collected from the water purification tank. Bar, 100 μm. (B) Enlarged spirally twisted stalks connected to a bean-shaped bacterial cell (arrowhead). Bar, 10 μm. (C) SEM image of a twisted stalk comprising of parallel-arranged fibers. Bar, 1 μm. (D) TEM image of the stalk elongating from the concave side of a bacterial cell (arrowhead). Bar, 500 nm.

groundwater receiving tank were collected from the freshwater purification pilot plant at the farm of Okayama University. The collected samples were washed repeatedly with sterilized ultrapure water. Although typical twisted stalks produced by *Gallionella ferruginea* were confirmed to be the predominant deposits in the flocs by using a differential interference contrast microscope (BX-51; Olympus), it was unavoidable that a sample under consideration could be a mixed population because natural product sampling was conducted in an open-air tank. For TEM, the specimens were collected by centrifugation and fixed on ice for 2 h with a mixture of 2.5% glutaraldehyde, 1% OsO_4, and 4.5% sucrose in 0.1 M cacodylate buffer (pH 7.4), followed by embedding in agar. Small pieces of washed agar block were stained with 0.5% aqueous uranyl acetate at room temperature for 30 min and then dehydrated in a graded series of ethanol before being embedded in Quetol 651 resin mixture (NEM, Japan). Ultrathin sections (70 nm) were cut from the resin blocks and mounted onto Cu grids for observation by a TEM (H-7100; Hitachi, Japan) operated at 80 kV.

For SEM analysis, a suspension of the washed specimens was dropped onto an Al stub and vacuum dried. The specimen was Pt coated and observed with an SEM (S-4300; Hitachi, Japan).

Washed specimens were also resuspended in 100% ethanol, mounted onto Cu grids precoated with an amorphous lacy carbon film, and air dried for HRTEM analyses. HRTEM, SAED, and STEM/secondary electron imaging (STEM/SEI) were performed using a TEM/STEM (JEM-2100F; JEOL, Japan) with spherical aberration (C_s) corrector (CEOS, Germany) operated at 200 kV. The C_s corrector was not employed for the TEM mode but for the STEM mode. Fast Fourier transformation (FFT) images were constructed using Gatan digital micrograph software.

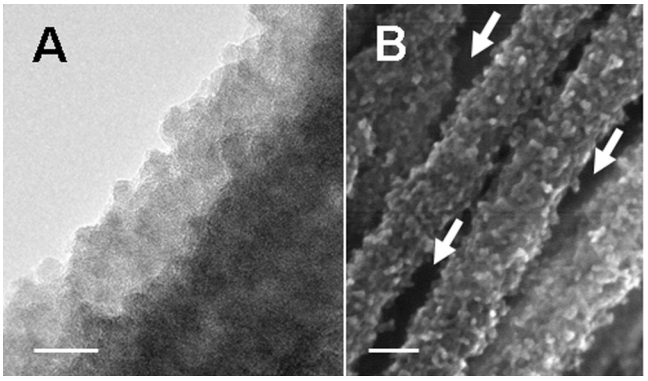

FIG 2 (A) HRTEM image of the fiber edge composed of nanometer-scale primary particles (~3 nm in diameter). Bar, 10 nm. (B) STEM/SEI image of the fibers with rough and granular surface. Arrows, interfiber spaces. Bar, 20 nm.

Pore distribution and specific surface detection. Nitrogen adsorption isotherms at 77 K were measured in liquid nitrogen baths by a Belsorp mini-II adsorption measurement instrument (Bel Japan, Inc.). Prior to measurement, the repeatedly washed and vacuum-dried sample was degassed *in vacuo* for 4 h at 100°C. The specific surface areas were calculated from the Brunauer-Emmett-Teller (BET) equation (2). Pore size distribution was calculated by Dollimore-Heal (DH) (13, 14) and micropore analysis (MP) (38) methods based on the desorption branch of the isotherms.

FTIR spectroscopy and powder XRD. FTIR spectra were recorded at room temperature on a Digilab FTS4000MXK FTIR spectrophotometer (Randolph) with a mercury-cadmium-telluride (MCT) detector maintained at the temperature of liquid N_2. A total of 144 detector readings were accumulated at a spectral resolution of 2 cm^{-1}. The sample (ca. 8 mg), vacuum dried as described above, was pressed into a 10-mm-diameter pellet.

The crystallinity of the same sample was evaluated by X-ray diffractometry (RINT-2000; Rigaku, Japan) using Cu Kα radiation (voltage, 40 kV; current, 200 mA). Scans were performed from 10° to 80° (2θ value) at a rate of 4° min^{-1} with a step size of 0.02°.

RESULTS AND DISCUSSION

The ocherous flocs collected for this study consisted predominantly of numerous spirally twisted stalks (Fig. 1A and B) and their associated bean-shaped bacterial cells (Fig. 1B, arrowhead). The twisted stalks consisted of many parallel-bundled fibers (Fig. 1C) that originated from the concave side of the bacterial cell (Fig. 1D, arrowhead). These features are consistent with earlier descriptions of *Gallionella ferruginea* (21, 25, 52).

An underfocused TEM image of the fiber matrix revealed assembled primary particles of ca. 3 nm in diameter at the fiber edge (Fig. 2A). These features are similar in morphology to the ca. 5-nm spherical clumps of ferrihydrite produced by cultured *Gallionella*, as observed by TEM imaging (4). The rough and granular surface of the fibers in the STEM/SEI image reflects the disordered assembly of the primary particles (Fig. 2B). Pore size distribution analyses of the fiber surface by the MP method for micropore analysis (pore diameter [d_p], <2 nm) and the DH method for mesopore analysis (pore radius [r_p], 2 to 50 nm) exhibited a wide distribution of a great number of micropores (mostly d_p of 1 nm) (Fig. 3A) and mesopores (r_p, <3 nm) (Fig. 3B) in the fiber. Such uneven

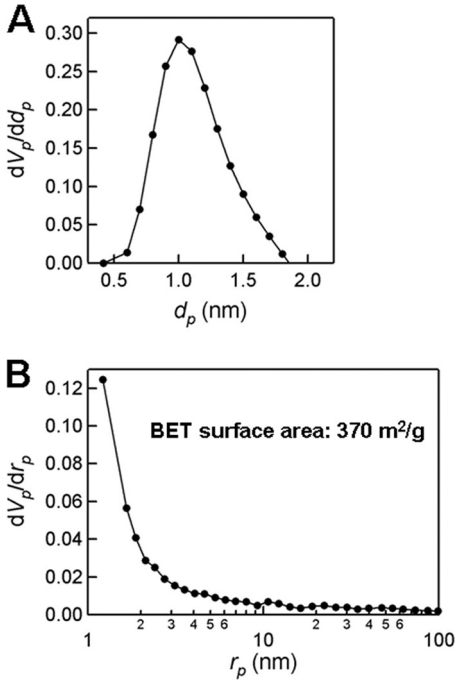

FIG 3 Pore size distribution profiles of the sample calculated by the MP method for micropore (A) and the DH method for mesopore (B).

surfaces together with the interfiber spaces (Fig. 2B, arrows) give rise to an extremely large specific surface area (BET surface area, 370 m^2/g). Emerson et al. (16) noted that the biogenic iron oxyhydroxides produced as a result of Fe oxidation by iron-oxidizing bacteria are always poorly crystalline forms of ferrihydrite, providing the important characteristics of large surface area, reactive surface properties, and the ability to be readily reduced. Such high porosity and large specific surface area of the stalk fibers could be a significant characteristic when we consider their industrial applications as a functional material.

The degree of crystallinity of the fibers was evaluated by XRD, SAED, and HRTEM. The XRD pattern with two broad peaks (Fig. 4A) and the TEM/SAED pattern with two halo rings corresponding to d-spacing values of 0.26 and 0.15 nm (Fig. 4B, inset) indicate a 2-line ferrihydrite, which is iron oxyhydroxide of a low crystallinity (29, 37). Ferris et al. (20) analyzed *Gallionella*-associated iron oxide precipitates by electron diffraction and found that their matrix gave weak diffuse patterns indicative of a poorly ordered material with very little long-range crystalline structure. Similarly, Søgaard et al. (50) analyzed *G. ferruginea* stalks by SAED and found that the Fe-encrusted fibers were amorphous, while the Fe-precipitated lumps were microcrystalline. On the basis of this analytical data, they considered that after oxidation, the amorphous Fe(III) hydroxides were partly retained in the stalks of the exopolymer and partly released to initiate crystallization as microcrystallites. Their analytical data are consistent with the description by Chan et al. (4), which stated that filaments of *G. ferruginea* stalks consisted of amorphous iron oxyhydroxide. The XRD and TEM/SAED results obtained in our study were consistent with these data. Figure 4C shows the just-focused HRTEM image of a fiber edge which gives an image of an almost homogeneous matrix. The fringes of the nanometer-scale particles similar

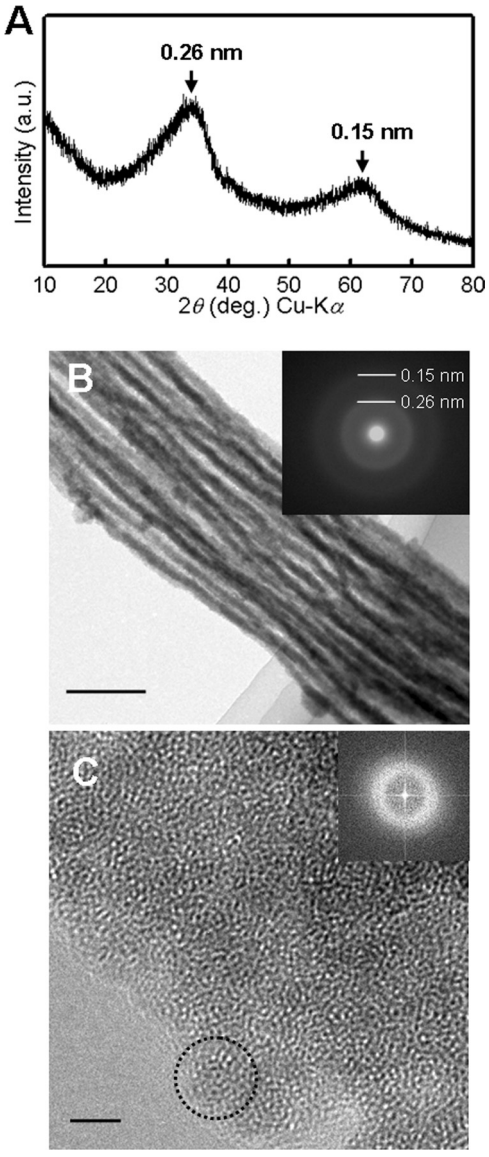

FIG 4 Evaluating the degree of crystallinity of the stalk fibers. (A) XRD pattern of the sample showing two broad peaks (d-spacing values of 0.26 and 0.15 nm). a.u., arbitrary units. (B) TEM image and its SAED pattern. Inset shows two halo rings corresponding to d-spacing values of 0.26 and 0.15 nm. Bar, 200 nm. (C) HRTEM image and its FFT pattern. Just-focused HRTEM image without lattice fringes reveals noncrystalline state of the matrix of a primary particle. Dot-lined circle corresponds to one primary particle when underfocused. Inset shows no spots caused by crystalline phase. Bar, 2 nm.

to those in Fig. 2A were observed in the same area as the underfocused image. The absence of lattice fringes in the highly magnified image (Fig. 4C) and the absence of spots, which would be caused by a crystalline phase, in the FFT pattern (Fig. 4C, inset) apparently indicate that the matrix of primary particles comprising the fiber has an amorphous structure.

As reported in previous EDX analytical data (52), Fe and O were the major elemental constituents of the fibers, and Si and P were minor elements, with an approximate atomic percentage ratio of Fe:Si:P = 79:16:5. As indicated in Table S1 in the supplemental material, the groundwater of the sampling site contains

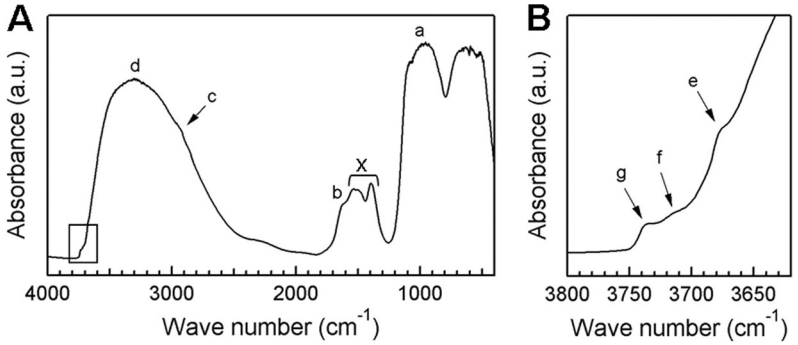

C

Index in figure	Wave number (cm^{-1})	Vibration mode
a	972	overlap of Si-O-Fe [7, 48, 49] and P-O-Fe [10, 22] stretching
b	1626	O-H bending [31,42]
c	2934	C-H stretching [31, 42]
d	3306	O-H stretching [31, 42]
e	3676	O-H stretching attached to P [8, 28]
f	3717	O-H stretching attached to Fe [28]
g	3736	O-H stretching attached to Si [47, 54, 58, 59]

FIG 5 (A and B) FTIR spectra of the sample. Band in squared area in panel A is enlarged in panel B. a.u., arbitrary units. (C) Alphabetical indices in panels A and B show vibration modes assigned to wave numbers, respectively, listed in the table. Superscript numbers in parentheses are reference numbers.

Ca, Na, Si, Fe, and Mg (all >10 μg/ml) and Mn and P (<2 μg/ml). Data evidently show that the concentrations of solutes in the groundwater do not account for those of the stalks, suggesting that Fe, Si, and P might be preferentially impregnated into the stalks, regardless of their contents in aquatic environments. To date, many researchers have performed EDX analysis on *Gallionella* stalks and have detected Fe, O, Si, Al, Ca, Cl, and/or P as the compositional elements, the ratios of which were largely affected by the bacterial states and habitats (5, 6, 24, 27, 32–34, 44, 52). However, all of these earlier papers consistently proved that Fe was the most prevalent, regardless of the environmental habitat of the bacteria. Suzuki et al. (52) showed by electron energy loss spectroscopy that the stalk fibers of *Gallionella* had a central carbon core of bacterial exopolymers and postulated that aquatic Fe could interact with O at the surface of the carbon core, resulting in deposition of iron oxides at the surface. These results were not inconsistent with the earlier report by Hallberg and Ferris (24) that in minute, flaky Fe precipitates within *Gallionella* fibers, the Fe/O atomic ratio was nearly 0.67 in individual crystallites, suggesting the stoichiometric formulation of Fe_2O_3. In addition, Chan et al. (4) demonstrated that *Gallionella* polysaccharides spatially correlated with iron oxyhydroxide distribution patterns as determined by X-ray fluorescence microscopy, suggesting that the organic fibrils could collect iron oxyhydroxide and control its recrystallization in the stalks. Thus, knowledge of the interaction of Fe with O in *Gallionella* stalks has been collected to some extent. Kennedy et al. (32) noted that the adsorption of Si to poorly ordered iron oxides inhibits their subsequent conversion to more-crystalline forms of iron oxides such as hematite and goethite and that conversion occurs to a more ordered structure in nonsilicified iron oxides by evolving adsorbed water. However, the distribution of minor elements such as Si and P in the fiber matrix and their linkages with Fe and/or O still remain to be elucidated.

Our previous nanometer-scale EDX mappings detected an almost uniform distribution of Fe, O, Si, and P in the entire fibers (see Fig. S1 in the supplemental material) (52). Commonly, in the structure of Fe(III) oxyhydroxide, which occurs through the Fe(III) hydrolysis reaction in the presence of SiO_4 or PO_4 anions, Fe exists as $Fe^{3+}(O, OH)_6$ octahedral units, while Si and P are present as $Si^{4+}O_4$ and $P^{5+}O_4$ tetrahedral units, respectively (11, 12, 36, 43, 45, 46). This information and the current HRTEM and EDX data led us to suspect that the putative four elements were distributed amorphously as these respective units in the primary particles of the fiber. However, how these units and/or individual elements interact with each other in the fiber matrix still remains in question. Thus, we set out to analyze the chemical linkages of Fe, O, Si, and P in the current sample by FTIR spectroscopy. The broad bands near 1,630 and 3,300 cm^{-1} are ascribed to O-H bending and stretching vibrations (31, 42), respectively (Fig. 5A, b and d). The small bands near 3,680 cm^{-1} (Fig. 5B, e), 3,720 cm^{-1} (Fig. 5B, f), and 3,740 cm^{-1} (Fig. 5B, g) are assigned to the O-H stretching vibrations of OH groups attached to P (8, 28), Fe (28), and Si (49, 54, 58, 59), respectively. The band near 1,000 cm^{-1} is assigned to overlapped bands of Si-O-Fe (7, 48, 49) and P-O-Fe (10, 22) stretching vibrations (Fig. 5A, a). These results indicate that the fibers contain a large amount of adsorbed water and hydroxyl groups, as suggested by Kennedy et al. (32), and that Fe binds not only to O but also to Si and P via O. In addition, the small band near 2,900 cm^{-1} at the right shoulder of the broad band centered at approximately 3,400 cm^{-1} (Fig. 5A, c) is assigned to C-H

stretching vibrations (31, 42), suggesting the presence of organic materials in the fibers, which is consistent with earlier reports (4, 6, 21, 24, 50, 52). Any references to assign the multiple bands between 1,300 and 1,580 cm^{-1} (Fig. 5A, x) have not yet been found. These results led us to suspect that $Fe^{3+}(O, OH)_6$, $Si^{4+}(O, OH)_4$, and $P^{5+}(O, OH)_4$ could exist as terminal groups of ionic linkages, probably at the surface of the primary particles, while $Fe^{3+}O_6$, $Si^{4+}O_4$, and $P^{5+}O_4$ units could connect each other randomly inside the particles. The previous EDX (see Fig. S1 in the supplemental material) and current FTIR showed that Fe, Si, P, and O and their associated linkages evidently existed in the stalks. However, because FTIR is a bulk measurement, the spatial associations of these constituents, for example, with the nanometersized ferrihydrite surface or interiors or secondary phases (e.g., amorphous SiO_2 and/or Fe phosphates) is ambiguous. Therefore, it is still too early to consider that the putative linkages exist uniformly in the entire fiber matrix including the interior.

As was reported earlier, inorganic ligands such as SiO_4 or PO_4 in Fe(III) hydrolysates could interfere with the polymerization and crystallization of Fe oxyhydroxide precipitates (9, 11, 46). Furthermore, organic materials are known to similarly affect the crystallization of Fe oxyhydroxide precipitates during hydrolysis (17, 39, 40). Although we must be more careful before reaching a significant conclusion about the chemical constitution of the fiber matrix, we still suspect that SiO_4, PO_4, and other minor elements in groundwater together with organic polymers of bacterial origin could greatly influence the construction of the fiber matrix comprising unique amorphous iron oxyhyrdoxides, which are distinct from the spontaneously formed siliceous ferrihydrite found in acid mine drainage (9) and the Si-doped ferrihydrite produced by artificial hydrolysis (49).

Many details remain unsolved in answering the question of whether Si and P interact with previously formed iron oxides, as was postulated by Kennedy et al. (32), or aquatic Fe(II) before oxidation and/or Fe(III) resulting from oxidation. Furthermore, some chemical bonds that clearly account for previously reported forms, FeOOH, α-FeOOH (4, 5, 6, 33), $Fe(OH)_3$ (20), and Fe_2O_3 (24), will be detected by other techniques. A further study of the interactions of organic molecules with the elements detected in this study will promote our basic understanding of the chemical character of *Gallionella* stalks. We fully agree with the invaluable observation of Emerson et al. (16) that understanding the structural details of these organomineral complexes will present an interesting interdisciplinary challenge for materials scientists, mineralogists, geochemists, and microbiologists.

ACKNOWLEDGMENTS

This study was financially supported by a Special Grant for Education and Research (2008.4-2013.3) from the Ministry of Education, Culture, Sports, Science, and Technology, Japan.

We are indebted to Tokuro Nanba, Graduate School of Environmental Science, Okayama University, for his critical reviewing and valuable suggestions.

REFERENCES

1. **Blöthe M, Roden EE.** 2009. Microbial iron redox cycling in a circumneutral-pH groundwater seep. Appl. Environ. Microbiol. **75**: 468–473.
2. **Brunauer S, Emmett PH, Teller E.** 1938. Adsorption of gasses in multimolecular layers. J. Amer. Chem. Soc. **60**:309–319.
3. **Bruneel O, et al.** 2011. Characterization of the active bacterial community involved in natural attenuation processes in arsenic-rich creek sediments. Microb. Ecol. **61**:793–810.
4. **Chan CS, Fakra SC, Edwards DC, Emerson D, Banfield JF.** 2009. Iron oxyhydroxide mineralization on microbial extracellular polysaccharides. Geochim. Cosmochim. Acta **73**:3807–3818.
5. **Chan CS, Fakra SC, Emerson D, Fleming EJ, Edwards KJ.** 2011. Lithotrophic iron-oxidizing bacteria produce organic stalks to control mineral growth: implication for biosignature formation. ISME J. **5**:717–727.
6. **Chan CS, et al.** 2004. Microbial polysaccharides template assembly of nanocrystal fibers. Science **303**:1656–1658.
7. **Chanéac C, Tronc E, Jolivet JP.** 1996. Magnetic iron oxide–silica nanocomposites. Synthesis and characterization. J. Mater. Chem. **6**:1905–1911.
8. **Cheng ZH, Yasukawa A, Kandori K, Ishikawa T.** 1998. FTIR study of adsorption of CO_2 on nonstoichiometric calcium hydroxyapatite. Langmuir **14**:6681–6686.
9. **Cismasu AC, Michel FM, Tcaciuc AP, Tyliszczak T, Brown GE, Jr.** 2011. Composition and structural aspects of naturally occurring ferrihydrite. C. R. Geosci. **343**:210–218.
10. **Daou TJ, et al.** 2007. Phosphate adsorption properties of magnetite-based nanoparticles. Chem. Mater. **19**:4494–4505.
11. **Doelsch E, et al.** 2000. Speciation and crystal chemistry of iron (III) chloride hydrolyzed in the presence of SiO_4 ligands. 1. An Fe K-edge EXAFS study. Langmuir **16**:4726–4731.
12. **Doelsch E, et al.** 2001. Speciation and crystal chemistry of iron (III) chloride hydrolyzed in the presence of SiO_4 ligands. 2. Characterization of Si-Fe aggregates by FTIR and ^{29}Si solid-state NMR. Langmuir **17**: 1399–1405.
13. **Dollimore D, Heal GR.** 1964. An improved method for the calculation of pore size distribution from adsorption data. J. Applied Chem. **14**: 109–114.
14. **Dollimore D, Heal GR.** 1970. Pore-size distribution in typical adsorbent systems. J. Colloid Interface Sci. **33**:508–519.
15. **Duckworth OW, Holmström SJM, Peña J, Sposito G.** 2009. Biogeochemistry of iron oxidation in a circumneutral freshwater habitat. Chem. Geol. **260**:149–158.
16. **Emerson D, Fleming EJ, McBeth JM.** 2010. Iron-oxidizing bacteria: an environmental and genomic perspective. Annu. Rev. Microbiol. **64**: 561–583.
17. **Eusterhues K, et al.** 2008. Characterization of ferrihydrite-soil organic matter coprecipitates by X-ray diffraction and Mössbauer spectroscopy. Environ. Sci. Technol. **48**:7891–7897.
18. **Ferris FG.** 2005. Biogeochemical properties of bacteriogenic iron oxides. Geomicrobiol. J. **22**:79–85.
19. **Ferris FG, Fyfe WS, Beveridge TJ.** 1987. Bacteria as nucleation sites for authigenic minerals in a metal-contaminated lake sediment. Chem. Geol. **63**:225–232.
20. **Ferris FG, Konhauser KO, Lyvén B, Pedersen K.** 1999. Accumulation of metals by bacteriogenic iron oxides in a subterranean environment. Geomicrobiol. J. **16**:181–192.
21. **Ghiorse WC.** 1984. Biology of iron- and manganese-depositing bacteria. Annu. Rev. Microbiol. **38**:515–550.
22. **Gunasekaran G, Chauhan LR.** 2004. Eco friendly inhibitor for corrosion inhibition of mild steel in phosphoric acid medium. Electrochim. Acta **49**:4387–4395.
23. **Hallbeck L, Pedersen K.** 1991. Autotrophic and mixotrophic growth of *Gallionella ferruginea.* J. Gen. Microbiol. **137**:2657–2661.
24. **Hallberg R, Ferris FG.** 2004. Biomineralization by *Gallionella.* Geomicrobiol. J. **21**:325–330.
25. **Hanert HH.** 2006. The genus *Gallionella.* Prokaryotes **7**:990–995.
26. **Hashimoto H, et al.** 2007. Characteristics of hollow microtubes consisting of amorphous iron oxide nanoparticles produced by iron oxidizing bacteria, *Leptothrix ochracea.* J. Magn. Magn. Mater. **310**:2405–2407.
27. **Heldal M, Tumyr O.** 1983. *Gallionella* from metalimnion in an eutrophic lake: morphology and X-ray energy-dispersive microanalysis of apical cells and stalks. Can. J. Microbiol. **29**:303–308.
28. **Ishikawa T, Saito H, Yasukawa A, Kandori K.** 1996. Adsorption of CO_2, CH_3OH, and H_2O on Fe(III)-substituted calcium hydroxyapatites. Bull. Chem. Soc. Jpn. **69**:899–907.
29. **Jambor JL, Dutrizac JE.** 1998. Occurrence and constitution of natural and synthetic ferrihydrite, a widespread iron oxyhydroxide. Chem. Rev. **98**:2549–2585.

30. **James RE, Ferris FG.** 2004. Evidence for microbial-mediated iron oxidation at a neutrophilic groundwater spring. Chem. Geol. **212**:301–311.
31. **Jitianu A, Crisan M, Meghea A, Rau I, Zaharescu M.** 2002. Influence of the silica based matrix on the formation of iron oxide nanoparticles in the Fe_2O_3-SiO_2 system, obtained by sol-gel method. J. Mater. Chem. **12**: 1401–1407.
32. **Kennedy CB, Scott SD, Ferris FG.** 2003. Ultrastructure and potential sub-seafloor evidence of bacteriogenic iron oxides from Axial Volcano, Juan de Fuca Ridge, north-east Pacific Ocean. FEMS Microbiol. Ecol. **43**: 247–254.
33. **Kennedy CB, Scott SD, Ferris FG.** 2004. Hydrothermal phase stabilization of 2-line ferrihydrite by bacteria. Chem. Geol. **212**:269–277.
34. **Langley S, et al.** 2009. Preliminary characterization and biological reduction of putative biogenic iron oxides (BIOS) from the Tonga-Kermadec Arc, southwest Pacific Ocean. Geobiology **7**:35–49.
35. **Li D, et al.** 2010. Characterization of bacterial community structure in a drinking water distribution system during an occurrence of red water. Appl. Environ. Microbiol. **76**:7171–7180.
36. **Masion A, Rose J, Bottero J-Y, Tchoubar D, Elemerich P.** 1997. Nucleation and growth mechanisms of iron oxyhydroxide in the presence of PO_4 ions. 3. Speciation of Fe by small angle X-ray scattering. Langmuir **13**:3882–3885.
37. **Michel FM, et al.** 2007. The structure of ferrihydrite, a nanocrystalline material. Science **316**:1726–1729.
38. **Mikhail RS, Brunauer S, Bodor EE.** 1968. Investigations of a complete pore structure analysis I. Analysis of microstructure. J. Colloid Interface Sci. **26**:45–53.
39. **Mikutta C, et al.** 2008. Synthetic coprecipitates of exopolysaccharides and ferrihydrite. Part I: characterization. Geochim. Cosmochim. Acta **72**: 1111–1127.
40. **Mikutta C.** 2011. X-ray absorption spectroscopy study on the effect of hydroxybenzoic acids on the formation and structure of ferrihydrite. Geochim. Cosmochim. Acta **75**:5122–5139.
41. **Miot J, et al.** 2009. Extracellular iron biomineralization by photoautotrophic iron-oxidizing bacteria. Appl. Environ. Microbiol. **75**: 5586–5591.
42. **Nakamoto K (ed).** 1997. Infrared and Raman spectra of inorganic and coordination compounds, 5th ed, p 88–95. John Wiley & Sons, Inc, New York, NY.
43. **Pokrovski GS, Schott J, Farges F, Hazemann J-L.** 2003. Iron (III)-silica interactions in aqueous solution: insight from X-ray absorption fine structure spectroscopy. Geochim. Cosmochim. Acta **67**:3359–3573.
44. **Ridgway HF, Olson BH.** 1981. Iron bacteria in drinking water distribution systems: elemental analysis of *Gallionella* stalks, using X-ray energy-dispersive microanalysis. Appl. Environ. Microbiol. **41**:288–297.
45. **Rose J, Flank A-M, Masion A, Bottero J-Y, Elmerich P.** 1997. Nucleation and growth mechanisms of Fe oxyhydroxide in the presence of PO_4 ions. 2. P K-edge EXAFS study. Langmuir **13**:1827–1834.
46. **Rose J, Manceau A, Bottero J-Y, Masion A, Garcia F.** 1996. Nucleation and growth mechanisms of Fe oxyhydroxide in the presence of PO_4 ions. 1. Fe K-edge EXAFS study. Langmuir **12**:6701–6707.
47. **Sakai T, et al.** 2010. Chemical modification of biogenous iron oxide to create an excellent enzyme scaffold. Org. Biomol. Chem. **8**:336–338.
48. **Scarano D, et al.** 1993. Fourier-transform infrared and Raman spectra of pure and Al-, B-, Ti- and Fe-substituted silicalites: stretching-mode region. J. Chem. Soc. Faraday Trans. **89**:4123–4130.
49. **Seehra MS, Roy P, Raman A, Manivannan A.** 2004. Structural investigations of synthetic ferrihydrite nanoparticles doped with Si. Solid State Commun. **130**:597–601.
50. **Søgaard EG, Medenwaldt R, Abraham-Peskir JV.** 2000. Conditions and rates of biotic and abiotic iron precipitation in selected Danish freshwater plants and microscopic analysis of precipitate morphology. Water Res. **34**:2675–2682.
51. **Spring S.** 2006. The genera *Leptothrix* and *Sphaerotilus.* Prokaryotes **5**:758–777.
52. **Suzuki T, et al.** 2011. Nanometer-scale visualization and structural analysis of the inorganic/organic hybrid structure of *Gallionella ferruginea* twisted stalks. Appl. Environ. Microbiol. **77**:2877–2881.
53. **Urrutia MM, Beveridge TJ.** 1994. Formation of fine-grained metal and silicate precipitates on a bacterial surface (*Bacillus subtilis*). Chem. Geol. **116**:261–280.
54. **Vansant EF, Van Der Voort P, Vrancken KC.** 1995. Chapter 3. The surface chemistry of silica. Stud. Surf. Sci. Catal. **93**:59–77.
55. **van Veen WL, Mulder EG, Deinema MH.** 1978. The *Sphaerotilus-Leptothrix* group of bacteria. Microbiol. Rev. **42**:329–356.
56. **Wang J, Muyzer G, Bodelier PLE, Laanbroek HJ.** 2009. Diversity of iron oxidizers in wetland soils revealed by novel 16S rRNA primers targeting Gallionella-related bacteria. ISME J. **3**:715–725.
57. **Wu Z, Yuan L, Jia N, Wang Y, Sun L.** 2009. Microbial biomineralization of iron seepage water: implication for the iron ores formation in intertidal zone of Zhoushan Archipelago, East China Sea. Geochem. J. **43**:167–177.
58. **Zecchina A, et al.** 1992. Silicalite characterization. 1. Structure, adsorptive capacity, and IR spectroscopy of the framework and hydroxyl modes. J. Phys. Chem. **96**:4985–4990.
59. **Zecchina A, et al.** 1992. Silicalite characterization. 2. IR spectroscopy of the interaction of CO with internal and external hydroxyl groups. J. Phys. Chem. **96**:4991–4997.